J. Fluid Mech. (2016), *vol.* 797, R1, doi:10.1017/jfm.2016.285

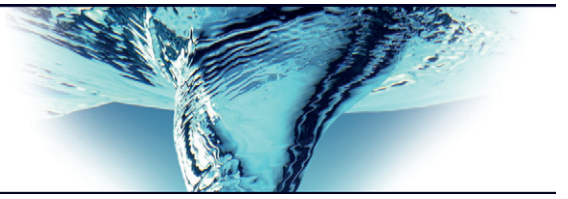

JFM RAPIDS
journals.cambridge.org/rapids

Turbulent/non-turbulent interfaces in wakes in stably stratified fluids

Tomoaki Watanabe[1,5,†], James J. Riley[1], Stephen M. de Bruyn Kops[2], Peter J. Diamessis[3] and Qi Zhou[4]

[1]Department of Mechanical Engineering, University of Washington, Seattle, WA 98195, USA

[2]Department of Mechanical and Industrial Engineering, University of Massachusetts Amherst, Amherst, MA 01003-9284, USA

[3]School of Civil and Environmental Engineering, Cornell University, Ithaca, NY 14853, USA

[4]Department of Applied Mathematics and Theoretical Physics, University of Cambridge, Cambridge CB3 0WA, UK

[5]Department of Aerospace Engineering, Nagoya University, Nagoya 464-8603, Japan

(Received 23 January 2016; revised 15 March 2016; accepted 17 April 2016)

We report on a study, employing direct numerical simulations, of the turbulent/non-turbulent interface of a wake in a stably stratified fluid. It is found that thresholds for both enstrophy and potential enstrophy are needed to identify the interface. Using conditional averaging relative to the location of the interface, various quantities of interest are examined. The thickness of the interface is found to scale with the Kolmogorov scale. From an examination of the Ozmidov and Kolmogorov length scales as well as the buoyancy Reynolds number, it is found that the buoyancy Reynolds number decreases and becomes of order 1 near the interface, indicating the suppression of the turbulence there by the stable stratification. Finally the overall rate of loss of energy due to internal wave radiation is found to be comparable to the overall rate of loss due to turbulent kinetic energy dissipation.

Key words: stratified turbulence, turbulent flows, wakes

1. Introduction

Turbulence in stably stratified fluids is usually localized, such as turbulence due to local breakdown of internal waves, turbulence in the ocean mixed layer, turbulence in a stably stratified atmospheric boundary layer, and in many other circumstances (e.g. Thorpe 2005). Therefore an interface exists between the turbulent and non-turbulent flows. Of considerable interest is the behaviour of the flow near this interface; this is where, for example, the turbulent region can grow into the

† Email address for correspondence: tomoakiw@uw.edu

non-turbulent region by entrainment, where mass, momentum and energy exchanges occur, and where internal waves are generated that propagate away from the turbulent region.

The behaviour of the turbulent/non-turbulent (T/NT) interface for non-stratified fluids is becoming much better understood, starting with the seminal work of Corrsin & Kistler (1955), who used laboratory experiments to explore T/NT interfaces in turbulent boundary layers, plane wakes and circular jets. A principal contribution of their research was conceptual. In order to distinguish the turbulent and non-turbulent regions they concluded that the essential characteristic of the turbulence was its high vorticity, and applied the word turbulence to 'random rotational fields'. Corrsin and Kistler used a configuration of four hot-wire probes to measure vorticity at a point as a function of time. More recently, optical methods have been used in the laboratory (Westerweel *et al.* 2002, 2009) and high-resolution direct numerical simulations have been performed (Taveira & da Silva 2014; Watanabe *et al.* 2015), both of which can produce a two- or three-dimensional snapshot of the flow field and hence much better information about the T/NT interface. These later studies have found that the interface consists of two layers. In agreement with Corrsin and Kistler, the thickness of the viscous superlayer, which is formed at the outer edge of the interface, is of the order of the Kolmogorov scale. In addition, an adjacent interior layer, the turbulent sublayer, has also been identified. An approach that has been particularly enlightening has been to examine the statistics of the flow, conditioned relative to the interfacial layer (Bisset, Hunt & Rogers 2002), revealing much of the near interfacial dynamics. More recent results on T/NT interfaces are contained in the review by da Silva *et al.* (2014).

A principal feature of non-turbulent regions outside turbulent flows in stably stratified fluids is the existence of internal waves that are generated by the turbulence and propagate away from the turbulent region. For example, Gilreath & Brandtl (1985) and Bonneton, Chomaz & Hopfinger (1993) have made detailed measurements of the internal waves generated by the turbulent wake of a sphere moving horizontally in a stratified fluid, while Abdilghanie & Diamessis (2013) have studied this flow by implicit large-eddy simulation. Both laboratory and numerical simulations were employed by Maffioli *et al.* (2014) to study the generation of internal waves by a localized, grid-generated region of turbulence. In the ocean internal waves are often observed below the mixed layer (Wijesekera & Dillon 1991; Moum, Paulson & Caldwell 1992; Munroe & Sutherland 2014) and above a turbulent bottom Eckman layer (Taylor & Sarkar 2007), while in the atmosphere internal waves are found in the stably stratified flow above the atmospheric boundary layer (Muschinski *et al.* 2001).

In a stratified fluid the flow outside the turbulent region can contain internal waves, which possess vorticity, and so vorticity cannot be used as the sole quantity to distinguish the turbulent and non-turbulent regions, and hence to identify the T/NT interface. Following the suggestion of Riley & Lelong (2000), potential vorticity should be useful in identifying the non-turbulent region, since internal waves carry no potential vorticity. Potential vorticity has been used successfully by Maffioli *et al.* (2014) in distinguishing the non-turbulent region from a localized turbulent one.

In this paper we use very high-resolution direct numerical simulations to study the turbulent wake of a sphere moving horizontally in a stably stratified fluid. In particular we utilize both vorticity and potential vorticity to separate the turbulent and non-turbulent regions, and examine the behaviour of the flow in the vicinity of the T/NT interface. In the next section we describe the methodology used to simulate the wake.

In the following sections we then describe the method to separate the turbulent and non-turbulent regions, determine the scaling for the thickness of the interface, and examine some features of the flow in the vicinity of the interface. In the final section we summarize our results.

2. Methodology used for numerical simulation

The simulation data analysed in this paper are produced with a combination of implicit large-eddy simulation (ILES) and direct numerical simulation (DNS), both using the Navier–Stokes equations subject to the Boussinesq approximation. First, an ILES of each wake is run for a very long time in a computational domain sufficiently deep and wide to allow for the radiation and near-field propagation of wake-radiated internal waves, and with fine enough resolution to capture most of the turbulent motions. Next, selected snapshots in time of the full wake velocity and density fields are interpolated onto a very high-resolution DNS grid and advanced in time until the small-scale motions are in quasi-equilibrium with respect to the large-scale motions.

Before giving details of the ILES and DNS, let us consider the efficacy of studying DNS snapshots initialized with ILES. Since the wakes discussed in this paper are at much higher Reynolds number than those measured in the laboratory, no direct validations of the current results are possible. However, the ILES methodology has been demonstrated to reproduce important characteristics of laboratory wakes at lower Reynolds number (Spedding 1997, 2002; Diamessis, Spedding & Domaradzki 2011). Additionally, Lalescu, Meneveau & Eyink (2013) find that turbulent motions at scales smaller than 20 times the Kolmogorov length scale, η, are slaved to the chaotic motions of the larger scales. So, provided the ILES is sufficiently resolved, the smaller scales of the DNS fill in without changing the larger scales. By comparing the DNS and ILES results, it is observed that the ILES grid spacing is never more than 20η. We conclude, therefore, that the DNS can be expected to produce the correct dynamics of the wakes considered.

The numerical method and configuration of the ILES are discussed in detail in Diamessis *et al.* (2011), Abdilghanie & Diamessis (2013) and Zhou (2015). Briefly, the computational domain is a box that is periodic in both horizontal directions and has free-slip top/bottom walls. A Cartesian coordinate system (x, y, z) is defined, with x in the direction of the sphere tow, z in the vertical direction, y in the horizontal direction perpendicular to x and z, and $(y, z) = (0, 0)$ is along the centreline of the wake. Sponge layers wrap around all of the boundaries of the domain, preventing the spurious re-entry and reflection of wake-radiated internal waves through the lateral and top/bottom boundaries, respectively. The flow is initialized to approximate the wake close behind a sphere without including the sphere in the computational domain. This is done by starting with the self-similar assumption of Meunier, Diamessis & Spedding (2006), which provides expressions for the initial streamwise-averaged mean and r.m.s.-fluctuating velocity profiles for chosen values of reference sphere diameter, D, and tow speed, U. The velocity field is initialized with random noise, which is windowed on the above profiles; then turbulence is allowed to develop over the course of a preliminary relaxation run in a background of homogeneous density. Following the progressive imposition of a constant mean density gradient, $\mathrm{d}\bar{\rho}/\mathrm{d}z$ with gravitational acceleration g, the wake flow field develops freely such that the mean velocity profile evolves according to the power laws observed in the laboratory (Spedding 1997, 2002). The spatial discretization of the numerical solution relies on a Fourier pseudospectral method in the horizontal directions and on a

Case	1	2
ILES dim.	$4 \times 6 \times 2.25$	$4 \times 2.0 \times 0.87$
DNS dim.	$4 \times 3 \times 0.75$	$4 \times 1.5 \times 0.75$
DNS points	$4096 \times 3072 \times 768$	$16\,384 \times 6144 \times 3072$
Re_L, $Nt = 11$	2.7×10^3	2.4×10^4
Re_L, $Nt = 21$	5.2×10^3	5.2×10^4

TABLE 1. Simulation parameters; dimensions are in metres. The diameter and tow speed of the reference sphere are $D = 0.15$ m and $U = 0.0336$ m s^{-1}. The Reynolds number in the simulations is changed by adjusting the kinematic viscosity ν. Here $Re_L = u'L/\nu$, where u' and L are the centreline r.m.s. axial velocity and the longitudinal integral scale of the axial velocity, respectively. The Prandtl number, $Pr = \nu/\kappa$ where κ is the mass diffusivity, is taken to be 1 in the DNS.

spectral multidomain penalty method based on Legendre polynomials in the vertical (Diamessis, Domaradzki & Hesthaven 2005). Numerical stability is maintained by the penalty method and by spectral filtering in all three spatial directions. It is this spectral filter that serves as a surrogate for a subgrid scale model in the ILES. As needed, the wake is gradually interpolated onto a larger domain with a coarser grid to accommodate the propagation of internal waves radiating from the turbulent core and also to prevent spurious interactions with the wake's spanwise periodic counterpart. The domain dimensions, and the Reynolds numbers for the cases and times considered, are given in table 1.

To initialize the DNS, snapshots of the ILES are taken at $Nt = 9$ and 19, and interpolated onto uniformly spaced grids with dimensions given in table 1. Here t is time, $N = \sqrt{-(g/\rho_0)(\mathrm{d}\bar{\rho}/\mathrm{d}z)}$ is the buoyancy frequency and ρ_0 a constant reference density. The times shown in the table are the end times after the snapshot has been advanced in time for $Nt = 2$ using the fully periodic pseudospectral scheme described in Hebert & de Bruyn Kops (2006). The resolution of the DNS is such that the maximum wavenumber (after dealiasing) times η is at least 3.0. This criterion is shown in de Bruyn Kops (2015) and the references therein to enable accurate local small-scale quantities and converged statistics of at least the fourth-order moments of the velocity and scalar fluctuations. The DNS are advanced in time for $Nt = 2$ because it is observed that all terms in the enstrophy equation are quasi-stationary (in the sense that the wake evolves in time) within $Nt = 1.5$ after the time the DNS is started.

3. Detection of the T/NT interface

For non-stratified flows, for which the T/NT interface is defined as that separating strong vortical from irrotational flow, many methods have been used to set a threshold value for vorticity magnitude that can then be used to determine the interface. For example, Taveira *et al.* (2013) have computed the total volume of a turbulent region as a function of the vorticity threshold ω_{th}. They found that a plateau exists in the total volume for a range of values of ω_{th}. By examining the turbulent region graphically, they found very little variation in the location of the T/NT interface as the threshold was varied throughout this range; this implied that the vorticity threshold could be located in this range, and the threshold could be used in determining the T/NT interface. This technique has since been employed successfully to detect the

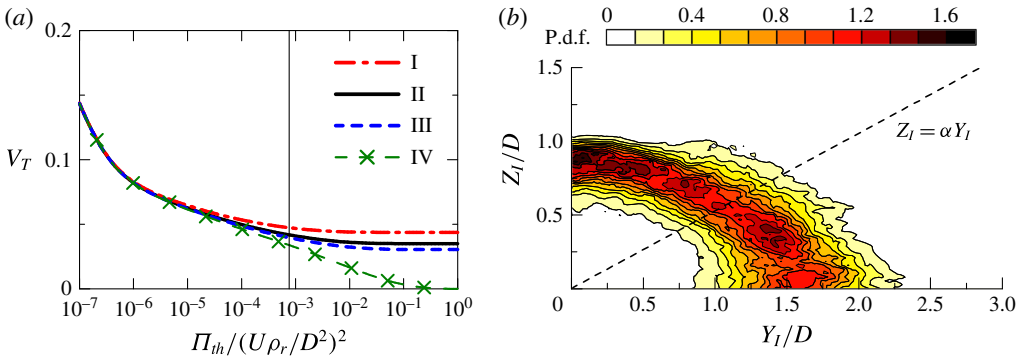

FIGURE 1. (*a*) Dependence of volume fraction of turbulent regions V_T on the threshold Π_{th} calculated at $Nt = 21$ (Case 1) for (I) $\omega_{th} = 0.05\langle\omega^2\rangle$, (II) $\omega_{th} = 0.1\langle\omega^2\rangle$, (III) $\omega_{th} = 0.15\langle\omega^2\rangle$ and (IV) $\omega_{th} = \infty$, where $\langle\omega^2\rangle$ is used as a reference value, with $\langle\cdot\rangle$ indicating the average along the centreline of the wake. The thresholds $\omega_{th} = 0.1\langle\omega^2\rangle$ and $\Pi_{th} = 0.023\langle\Pi^2\rangle$ are used for detecting turbulent regions. The vertical solid line in the figure indicates the threshold $\Pi_{th} = 0.023\langle\Pi^2\rangle$. (*b*) Joint p.d.f. of the location of the wake edge (Y_I, Z_I) at $Nt = 21$ for Case 1. The broken line in panel (*b*) shows $Z_I = \alpha Y_I$, where $\alpha = \langle Z_I\rangle/\langle Y_I\rangle$ is the aspect ratio defined by the mean locations of the wake edges $\langle Y_I\rangle$ at $z = 0$ and $\langle Z_I\rangle$ at $y = 0$.

T/NT interface in studies using direct numerical simulation of planar turbulent jets (Watanabe *et al.* 2014) and turbulent mixing layers (Attili, Cristancho & Bisetti 2014).

We here extend this method of identifying the T/NT interface to stably stratified flows by using, in addition to vorticity, the potential vorticity defined as $\Pi = \omega \cdot \nabla\rho$, where ω is the vorticity and ρ is the density. Potential vorticity satisfies the equation

$$\frac{\mathrm{D}\Pi}{\mathrm{D}t} = \frac{1}{Re}\frac{\partial}{\partial x_k}\left(g_i\frac{\partial\omega_i}{\partial x_k} + \frac{1}{Pr}\omega_i\frac{\partial g_i}{\partial x_k}\right) - \frac{1}{Re}\left(1 + \frac{1}{Pr}\right)\frac{\partial\omega_i}{\partial x_k}\frac{\partial g_i}{\partial x_k}, \tag{3.1}$$

where $g_i \equiv \partial\rho/\partial x_i$ and $\mathrm{D}/\mathrm{D}t$ is the usual substantial derivative. Here the equation has been non-dimensionalized using the sphere diameter D, tow speed U and a reference density $\rho_r = -D(\mathrm{d}\overline{\rho}/\mathrm{d}z)$. Neglecting viscous and diffusive effects, Π is conserved following the flow. This implies that, in a turbulent region for which the external flow is initially irrotational, the irrotational flow can only obtain potential vorticity by viscous and diffusive effects, and in particular not by internal wave propagation. The internal wave region outside the turbulent wake, therefore, although it contains vorticity through the propagation of the internal waves, can contain no potential vorticity.

Thresholds are simultaneously applied for both the vorticity squared (enstrophy) and the potential vorticity squared (potential enstrophy), and the vorticity/potential vorticity (turbulent) region is computed as a function of both thresholds. In particular, a local region is considered turbulent if either $\omega^2 > \omega_{th}$ or $\Pi^2 > \Pi_{th}$. In doing so a plateau is found, as a function of both variables, where the turbulent volume is somewhat insensitive to variations in both. Figure 1(*a*) is a typical plot, here for Case 1 at $Nt = 21$, of the volume fraction of the turbulent region as a function of the potential enstrophy threshold for a range of enstrophy thresholds. It is seen that indeed a significant plateau region does exist. Using this approach the core regions of the

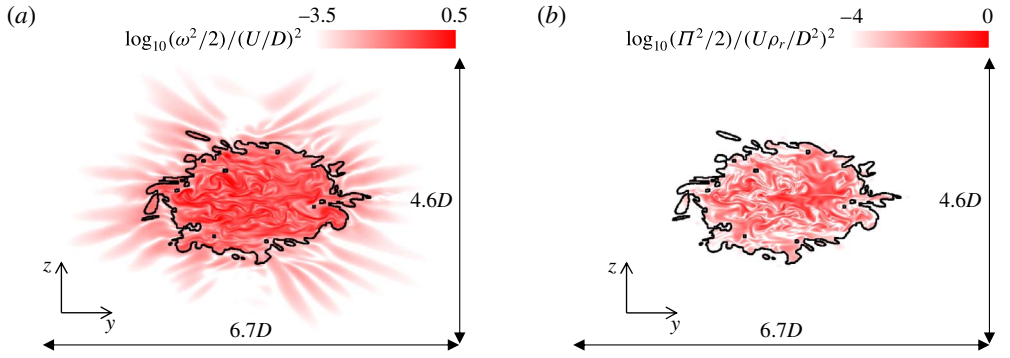

FIGURE 2. Vertical cross-sections of (*a*) enstrophy and (*b*) potential enstrophy fields at $Nt = 21$ for Case 1. The solid black line shows the wake edge.

wake are detected by vorticity whereas the wake edge is detected by potential vorticity. The wake edge identified based on the thresholds is located within the T/NT interface layer, and is used for investigating the flows near the interface.

Figure 1(*b*) gives the joint probability density (p.d.f.) function of the location of the wake edge on cross-sectional (y–z) planes for the same case and time. The plot shows how the turbulent region spreads more horizontally than vertically, and gives some idea of the spatial variation of the turbulent boundary along the length of the wake. Some perspective on the enstrophy and potential enstrophy fields, along with the use of the T/NT detection criterion, can be seen in figure 2(*a*,*b*), which are cross-sectional plots of enstrophy and potential enstrophy for a typical cross-plane for this same case. In figure 2(*a*) giving the enstrophy, both the turbulent wake region and the internal wave region are easily identified. In figure 2(*b*) the potential enstrophy region is seen to be very compact, and well defined by the T/NT detection scheme.

4. Results conditioned on the location of the interface

Having developed a method for detecting the T/NT interface, it is of interest to examine the behaviour of the flow properties in the vicinity of this interface. This is done by considering averages, conditioned on the location from the wake edge, $\langle * \rangle_I$. In the results presented here, the entire interface, along the length of the wake and around its circumference, is used for conditioning. Figure 3(*a*,*b*) give plots of the conditional enstrophy and potential enstrophy, respectively, where $r_I = 0$ is the location of the interface, r_I positive indicates the region outside the wake and r_I negative indicates the region inside the wake. r_I is taken in the radial direction. The dependences of the enstrophy and potential enstrophy on the Reynolds number and on decay time are clearly visible, as well as the sharp decrease in both quantities across the interface. In addition it is seen that the potential enstrophy decays much more rapidly with distance away from the turbulent region, as expected from the discussion of (3.1).

Of fundamental importance is the thickness of the interface itself. To determine this the conditional potential enstrophy, normalized by its value at the T/NT interface ($r_I = 0$), was plotted versus r_I scaled by several potentially relevant length scales. Figure 3(*c*) is a plot of the conditional potential enstrophy versus r_I scaled by the Kolmogorov length scale. The data collapse rather well, indicating that the width

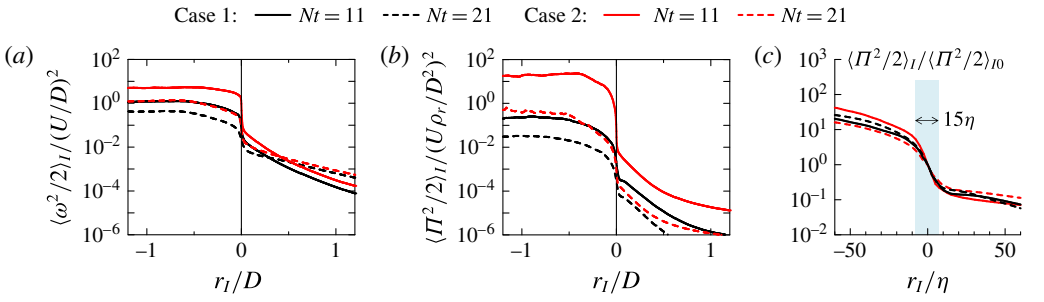

FIGURE 3. Conditional mean profiles of (*a*) enstrophy $\omega^2/2$ and (*b*) potential enstrophy $\Pi^2/2$. (*c*) Conditional mean potential enstrophy $\Pi^2/2$ against the distance from the wake edge normalized by the Kolmogorov length scale η. In (*c*), the conditional mean potential enstrophy is normalized by the value at the wake edge $\langle\Pi^2/2\rangle_{I0}$ at $r_I = 0$.

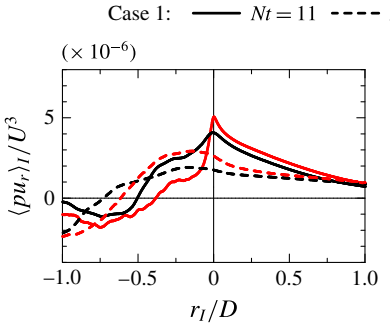

Case	Nt	ϵ_T	F_T
1	11	4.10×10^{-5}	2.58×10^{-5}
1	21	1.37×10^{-5}	1.34×10^{-5}
2	11	2.01×10^{-5}	2.79×10^{-5}
2	21	0.55×10^{-5}	1.67×10^{-5}

FIGURE 4. Conditional averaged profiles of the radial energy flux pu_r. The line types are the same as in figure 3. The table shows values of the total kinetic energy dissipation rate ϵ_T and the total energy flux F_T normalized by U_0 and D.

of the T/NT interface scales with the Kolmogorov length scale, the same result as for the non-stratified case (Watanabe *et al.* 2015). In both cases the turbulent region grows into the non-turbulent region by the diffusion of vorticity; this diffusion process depends on the fluid viscosity ν as well as on the local strain rate, of order $(\epsilon/\nu)^{1/2}$, leading dimensionally to the dependence on the Kolmogorov scale $\eta = (\nu^3/\epsilon)^{1/4}$.

Of particular interest is the rate at which energy is being lost from the turbulent wake in the form of internal waves. Assuming the existence of internal waves, the pressure–velocity product pu_i determines the energy flux of the internal waves in the x_i direction. Figure 4 is a plot of the conditional radial energy flux for the four cases considered. For the early time, at $Nt = 11$, the energy flux is very similar for the two cases of different Reynolds number, indicating some insensitivity to the Reynolds number. When the kinetic energy equation is integrated over the turbulent wake region, the term $\epsilon_T = (1/L_x)\int_{\mathscr{V}} \epsilon \, \mathrm{d}V$ represents the rate at which kinetic energy is being lost to heat per unit length of wake, while the term $F_T = L_p\langle pu_r\rangle_I$ represents the conditional energy flux per unit length across the wake boundary. Here $\mathscr{V}$ is the wake volume, L_x is the simulation length in the direction of the tow and L_p is the length of the perimeter of the average cross-section of the wake, assuming that the mean wake is of approximately elliptical shape with the minor and major radii of $\langle Z_I\rangle$ and $\langle Y_I\rangle$ and the aspect ratio α in figure 1(*b*). The table in figure 4 contains the values of both ϵ_T

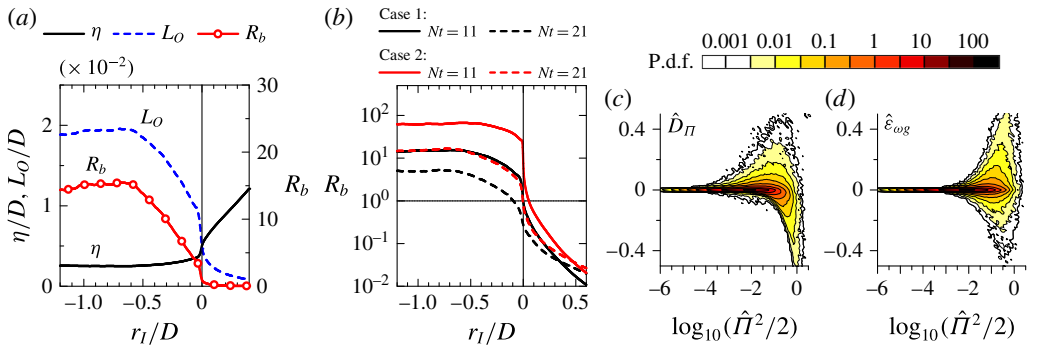

FIGURE 5. Conditional statistics of turbulence characteristics near the wake edge: (*a*) Kolmogorov length scale η, Ozmidov length scale L_O and buoyancy Reynolds number R_b calculated from the conditional mean dissipation rate of kinetic energy $\langle\epsilon\rangle_I$ at $Nt = 11$ for Case 1 and (*b*) logarithmic plots of buoyancy Reynolds number. (*c*) Conditional joint p.d.f. of potential enstrophy $\Pi^2/2$ and the viscous/molecular-diffusion term D_Π at $r_I/D = -0.1$. (*d*) Conditional joint p.d.f. of potential enstrophy $\Pi^2/2$ and the production/dissipation term $\epsilon_{\omega g}$ at $r_I/D = -0.1$. The results at $Nt = 11$ for Case 1 are presented. In this figure, the hats denote variables normalized by U_0, D and $\rho_r = D(-\mathrm{d}\overline{\rho}/\mathrm{d}z)$.

and F_T. Note that the values are very similar, especially at the later times and for the case of higher Reynolds number. These results indicate that the energy loss to internal wave radiation is of the same order as that lost due to the dissipation of kinetic energy into heat.

To determine the strength of the turbulence in the wake, of particular interest is the behaviour of both the Ozmidov scale $L_O = (\epsilon/N^3)^{1/2}$ and the Kolmogorov scale η, and their ratio in terms of the buoyancy Reynolds number $R_b = (L_O/\eta)^{4/3} = \epsilon/\nu N^2$. The Ozmidov scale is often interpreted as the largest horizontal scale that can overturn in a turbulent flow in a stably stratified fluid (see e.g. Riley & Lindborg 2013). Gibson (1980) has argued that three-dimensional turbulence cannot exist when R_b is sufficiently small. In figure 5(*a*) are plotted both the conditional Ozmidov and Kolmogorov length scales as well as the buoyancy Reynolds number for Case 1 at the time $Nt = 11$. Three regions are visible in the plots. First of all, in the interior of the wake, for r_I/D less than about -0.5, all three parameters are somewhat uniform, indicative of an active turbulent region. Nearer the wake edge, in the range of about $-0.5 \leqslant r_I/D \leqslant 0$, both the Ozmidov scale and the buoyancy Reynolds number decrease monotonically, possibly indicating the existence of internal waves as well as turbulence. At about the wake edge, the Ozmidov and Kolmogorov scales become about equal, indicating the suppression of the turbulence at the wake edge. The buoyancy Reynolds number is then effectively zero outside the wake. The values of the buoyancy Reynolds number are plotted for all four cases in figure 5(*b*). Again the dependences on the Reynolds number and the decay time are clearly evident. At the earlier times, and at later times for Case 2, R_b is sufficiently large inside the wake, above a value of about 20 (Rohr *et al.* 1988; Ivey & Imberger 1991; Itsweire *et al.* 1993), that the turbulence is probably actively mixing. At the later time for Case 1, however, R_b has dropped below 10, which indicates that the flow is probably not exhibiting active mixing.

It is of interest to examine the behaviour near the T/NT interface of the potential enstrophy itself, $\Pi^2/2$. For this case with $Pr = 1$, multiplying (3.1) by Π and rearranging gives the equation for the potential enstrophy:

$$\frac{\mathrm{D}}{\mathrm{D}t}\Pi^2/2 = \frac{1}{Re}\nabla^2\Pi^2/2 - \frac{1}{Re}\boldsymbol{\nabla}\Pi\cdot\boldsymbol{\nabla}\Pi - \frac{2}{Re}\Pi\boldsymbol{\nabla}\omega_i\cdot\boldsymbol{\nabla}g_i. \tag{4.1}$$

The first term on the right-hand side is the viscous/molecular-diffusion term, D_Π, the second is the dissipation-rate term, ϵ_Π, while the third is a mixed production/dissipation term, $\epsilon_{\omega g}$. The latter term can take on either sign. Some idea of the behaviour of these terms is found in figure 5(*c*,*d*), which give conditional joint probability density functions of D_Π and $\Pi^2/2$, and of $\epsilon_{\omega g}$ and $\Pi^2/2$, respectively. These two figures are taken from Case 1 at $Nt = 11$, and at the location inside the wake of $r_I/D = -0.1$, but are representative of plots of the same quantities at other points in the wake turbulence. From figure 5(*c*) one sees, in particular, that for low values of $\Pi^2/2$, the fluid acquires potential enstrophy primarily by viscous/molecular diffusion. For larger values of $\Pi^2/2$, potential enstrophy is both increased and decreased by viscous/molecular diffusion, but D_Π tends to negative values for very large $\Pi^2/2$, indicating the transport of potential enstrophy from the turbulent wake region with large $\Pi^2/2$ to the entrained fluid with small $\Pi^2/2$. From figure 5(*d*) one sees that the joint production/dissipation term $\epsilon_{\omega g}$, representing the effects of molecular diffusion on the alignment of ω_i and $\boldsymbol{\nabla}\rho$, takes on both positive and negative values, is effective at larger values of $\Pi^2/2$ and has a preference for positive values.

Since the isosurface of potential enstrophy is used for detecting the wake edge, the local entrainment velocity v_e (Holzner & Lüthi 2011) is obtained as the propagation velocity of the isosurface, $v_e = (\mathrm{D}\Pi^2/\mathrm{D}t)/|\boldsymbol{\nabla}\Pi^2|$. We find that the average value of v_e is very near zero for all four cases. Average entrainment velocities of the order of the Kolmogorov velocity have been found in non-stratified shear flows (Wolf *et al.* 2013; Watanabe *et al.* 2016). It appears that, for these later times in the wake (2–3 buoyancy periods), the stratification is inhibiting entrainment across the T/NT interface.

5. Conclusions

We have studied turbulent wakes in a stably stratified fluid using direct numerical simulations. For two cases, each at different Reynolds number, the wake is first simulated on a moderately large computational grid using an implicit large-eddy simulation. For each case and at two different points in time, the result is then mapped onto a grid of much higher resolution, and the simulations are carried out further in time with no modelling, all the scales of motion being well resolved. Using the output from the simulations, we first of all develop criteria to determine the turbulent/non-turbulent interface based upon both the enstrophy and the potential enstrophy. In particular, although the enstrophy is finite in the internal wave region, the potential enstrophy is essentially zero there, enabling the separation of the turbulent and non-turbulent regions. Using averaging conditioned on the location of the wake edge, it is then found that the interface thickness scales with the Kolmogorov scale, just as in the non-stratified case. Furthermore the Ozmidov scale, the Kolmogorov scale and the buoyancy Reynolds number, conditioned on the location relative to the wake edge, are examined both inside and outside the turbulent wake. It is found, as expected, that the buoyancy Reynolds number falls to order 1 near the wake edge, indicating the suppression of the turbulence there. In addition it is found that the

total energy flux from the wake at the T/NT interface is of the same order as the total dissipation rate of kinetic energy in the wake, indicating the importance of internal wave radiation to the overall behaviour of the wake. These latter results may have important implications regarding turbulence modelling, in that accurately simulating both the local buoyancy Reynolds number and internal wave radiation may be critical in properly modelling the wake. Finally, it is found that, in regions of very small potential enstrophy, the fluid receives potential enstrophy by viscous/molecular diffusion. For large values of the potential vorticity, the mixed production/dissipation term is found to take on both positive and negative values, although for larger values of Π^2 there is a preference for positive values (production).

Acknowledgements

Support through Office of Naval Research grants N00014-08-1-0235, N00014-13-1-0665 and N00014-15-12248, administered by Dr R. Joslin, is gratefully acknowledged. High performance computing resources were provided through the US Department of Defense High Performance Computing Modernization Program by the Army Engineering Research and Development Center and the Army Research Laboratory under Frontier Project FP-CFD-FY14-007.

References

ABDILGHANIE, A. M. & DIAMESSIS, P. J. 2013 The internal gravity wave field emitted by a stably stratified turbulent wake. *J. Fluid Mech.* **720**, 104–139.

ATTILI, A., CRISTANCHO, J. C. & BISETTI, F. 2014 Statistics of the turbulent/non-turbulent interface in a spatially developing mixing layer. *J. Turbul.* **15** (9), 555–568.

BISSET, D. K., HUNT, J. C. R. & ROGERS, M. M. 2002 The turbulent/non-turbulent interface bounding a far wake. *J. Fluid Mech.* **451**, 383–410.

BONNETON, P., CHOMAZ, J. M. & HOPFINGER, E. J. 1993 Internal waves produced by the turbulent wake of a sphere moving horizontally in a stratified fluid. *J. Fluid Mech.* **254**, 23–40.

DE BRUYN KOPS, S. M. 2015 Classical turbulence scaling and intermittency in stably stratified Boussinesq turbulence. *J. Fluid Mech.* **775**, 436–463.

CORRSIN, S. & KISTLER, A. L. 1955 Free-stream boundaries of turbulent flows. *NACA Tech. Rep.* **1224**, 1033–1064.

DIAMESSIS, P. J., DOMARADZKI, J. A. & HESTHAVEN, J. S. 2005 A spectral multidomain penalty method model for the simulation of high Reynolds number localized incompressible stratified turbulence. *J. Comput. Phys.* **202**, 298–322.

DIAMESSIS, P. J., SPEDDING, G. R. & DOMARADZKI, J. A. 2011 Scaling and structure of stably stratified wakes at high Reynolds number. *J. Fluid Mech.* **671**, 52–95.

GIBSON, G. H. 1980 Fossil temperature, salinity, and vorticity in turbulence in the ocean. *Marine Turbul.* 221–256.

GILREATH, H. E. & BRANDTL, A. 1985 Experiments on the generation of internal waves in a stratified fluid. *AIAA J.* **23** (5), 693–700.

HEBERT, D. A. & DE BRUYN KOPS, S. M. 2006 Predicting turbulence in flows with strong stable stratification. *Phys. Fluids* **18** (6), 1–10.

HOLZNER, M. & LÜTHI, B. 2011 Laminar superlayer at the turbulence boundary. *Phys. Rev. Lett.* **106** (13), 134503.

ITSWEIRE, E. C., KOSEFF, J. R., BRIGGS, D. A. & FERZIGER, J. H. 1993 Turbulence in stratified shear flows: implications for interpreting shear-induced mixing in the ocean. *J. Phys. Oceanogr.* **23**, 1508–1522.

IVEY, G. N. & IMBERGER, J. 1991 On the nature of turbulence in a stratified fluid. Part I: the energetics of mixing. *J. Phys. Oceanogr.* **21**, 650–658.

LALESCU, C. C., MENEVEAU, C. & EYINK, G. L. 2013 Synchronization of chaos in fully developed turbulence. *Phys. Rev. Lett.* **110**, 084102.

MAFFIOLI, A., DAVIDSON, P. A., DALZIEL, S. B. & SWAMINATHAN, N. 2014 The evolution of a stratified turbulent cloud. *J. Fluid Mech.* **739**, 229–253.

MEUNIER, P., DIAMESSIS, P. J. & SPEDDING, G. R. 2006 Self-preservation in stratified momentum wakes. *Phys. Fluids* **18**, 106601.

MOUM, J. N., PAULSON, C. A. & CALDWELL, D. R. 1992 Turbulence and internal waves at the equator. Part I: statistics from towed thermistors and a microstructure profiler. *J. Phys. Oceanogr.* **22**, 1330–1345.

MUNROE, J. R. & SUTHERLAND, B. R. 2014 Internal wave energy radiated from a turbulent mixed layer. *Phys. Fluids* **26**, 096604.

MUSCHINSKI, A., CHILSON, P. B., PALMER, R. D., HOOPER, D. A., SCHMIDT, G. & STEINHAGEN, H. 2001 Boundary-layer convection and diurnal variation of vertical-velocity characteristics in the free atmosphere. *Q. J. R. Meteorol. Soc.* **127**, 423–443.

RILEY, J. J. & LELONG, M. P. 2000 Fluid motions in the presence of strong stable stratification. *Annu. Rev. Fluid Mech.* **32**, 613–657.

RILEY, J. J. & LINDBORG, E. 2013 Recent progress in stratified turbulence. In *Ten Chapters in Turbulence* (ed. P. A. Davidson, Y. Kaneda & K. R. Sreenivasan), pp. 269–317. Cambridge University Press.

ROHR, J. J., ITSWEIRE, E. C., HELLAND, K. N. & VAN ATTA, C. W. 1988 Growth and decay of turbulence in a stably stratified shear flow. *J. Fluid Mech.* **195**, 77–111.

DA SILVA, C. B., HUNT, J. C. R., EAMES, I. & WESTERWEEL, J. 2014 Interfacial layers between regions of different turbulence intensity. *Annu. Rev. Fluid Mech.* **46**, 567–590.

SPEDDING, G. R. 1997 The evolution of initially turbulent bluff-body wakes at high internal Froude number. *J. Fluid Mech.* **337**, 283–301.

SPEDDING, G. R. 2002 Vertical structure in stratified wakes with high initial Froude number. *J. Fluid Mech.* **454**, 71–112.

TAVEIRA, R. R., DIOGO, J. S., LOPES, D. C. & DA SILVA, C. B. 2013 Lagrangian statistics across the turbulent–nonturbulent interface in a turbulent plane jet. *Phys. Rev.* E **88** (4), 043001.

TAVEIRA, R. R. & DA SILVA, C. B. 2014 Characteristics of the viscous superlayer in shear free turbulence and in planar turbulent jets. *Phys. Fluids* **26** (2), 021702.

TAYLOR, J. R. & SARKAR, S. 2007 Internal gravity waves generated by a turbulent bottom Eckman layer. *J. Fluid Mech.* **590**, 331–354.

THORPE, S. A. 2005 *The Turbulent Ocean*. Cambridge University Press.

WATANABE, T., SAKAI, Y., NAGATA, K., ITO, Y. & HAYASE, T. 2014 Vortex stretching and compression near the turbulent/nonturbulent interface in a planar jet. *J. Fluid Mech.* **758**, 754–785.

WATANABE, T., SAKAI, Y., NAGATA, K., ITO, Y. & HAYASE, T. 2015 Turbulent mixing of passive scalar near turbulent and non-turbulent interface in mixing layers. *Phys. Fluids* **27** (8), 085109.

WATANABE, T., DA SILVA, C. B., YASUHIKO, S., NAGATA, K. & HAYASE, T. 2016 Lagrangian properties of the entrainment across turbulent/non-turbulent interface layers. *Phys. Fluids* **27**, 031701.

WESTERWEEL, J., FUKUSHIMA, C., PEDERSEN, J. M. & HUNT, J. C. R. 2009 Momentum and scalar transport at the turbulent/non-turbulent interface of a jet. *J. Fluid Mech.* **631**, 199–230.

WESTERWEEL, J., HOFMANN, T., FUKUSHIMA, C. & HUNT, J. C. R. 2002 The turbulent/non-turbulent interface at the outer boundary of a self-similar turbulent jet. *Exp. Fluids* **33** (6), 873–878.

WIJESEKERA, H. W. & DILLON, T. M. 1991 Internal waves and mixing in the upper equatorial Pacific ocean. *J. Geophys. Res.* **96** (C4), 7115–7125.

WOLF, M., HOLZNER, M., LÜTHI, B., KRUG, D., KINZELBACH, W. & TSINOBER, A. 2013 Effects of mean shear on the local turbulent entrainment process. *J. Fluid Mech.* **731**, 95–116.

ZHOU, Q. 2015 Far-field evolution of turbulence-emitted internal waves and Reynolds number effects on a localized stratified turbulent flow, PhD thesis, Cornell University.